Technical report; TR-195

KNMI

ECBILT

A coupled Atmosphere Ocean Sea-ice model for climate predictability studies

R.J. Haarsma, F.M. Selten, J.D. Opsteegh, G. Lenderink and Q. Liu

De Bilt, 1996

Technical report = technisch rapport; TR-195

De Bilt, 1996

P.O. Box 201
3730 AE De Bilt
Wilhelminalaan 10
Telefoon 030-220 69 11
telefax 030-221 04 07

Auteurs: R.J. Haarsma, F.M. Selten,
J.D. Opsteegh, G. Lenderink
and Q. Liu

UDC: 551.583
551.526.63
551. 509.33
551.588.5

ISSN: 0169-1708

ISBN: 90-369-2115-5

● ● ● ●

ERRATUM

KNMI Technical Report, No. TR-195, entitled "ECBILT, A coupled Atmosphere Ocean Sea-ice model for climate predictability studies" by R.J. Haarsma, F.M. Selten, J.D. Opsteegh, G. Lenderink and Q. Liu.

Acknowledgements

This subproject was partly carried out, in the framework of the Dutch National Research Programme on Global Air Pollution and Climate Change, registered under No. 951208, titled: Climate Variability on Decadal Timescales.

ECBILT

A coupled Atmosphere Ocean Sea-ice model for climate predictability studies

R.J. Haarsma F.M. Selten J.D. Opsteegh
G. Lenderink Q. Liu
KNMI, De Bilt, The Netherlands

December 3, 1996

1 Introduction

The eventual detection of the antropogenic climate changes will be based on a clear picture of the characteristic behaviour of the climate system. The variability properties of both ocean and atmospheric models have been investigated in many papers using models of various complexity ranging from simple energy balance type models (EBM) to full GCMs. The thermohaline circulation of the oceans is believed to play an important role in determining the natural variability of the earth's climate(Bjerknes 1964, Broecker et al 1985, Stocker and Mysak 1992). Ocean models exhibit characteristic timescales of the order of ten to several hundreds of years which are connected to horizontal and vertical overturning transports of salt and heat (Weaver and Sarachik 1991, Mikolajewicz and Maier-Reimer 1990). From paleoclimatological data there is evidence that the conveyor belt in the ocean has indeed been disrupted from time to time. The best known example is the Younger Dryas Event. Approximately ten thousand years ago a sudden cooling occurred on a timescale of hundred years, connected to a significant decrease in the thermohaline circulation and poleward heattransport in the North-Atlantic. Broecker et al (1985) have suggested that this may be interpreted as a transition between different equilibrium states of the ocean circulation. The existence of multiple equilibrium states in ocean models has been shown in various papers (Bryan 1986, Manabe and Stouffer 1988, Marotzke and Willebrand 1991). The underlying mechanism is simple and has been demonstrated with conceptual models of the ocean (Stommel 1961). It appears that transitions between stationary equilibrium states can be triggered easily with moderate perturbations in the surface fluxes (Marotzke and Willebrand 1991, Maier-Reimer and Mikolajewicz 1989, Lenderink and Haarsma 1994). Regular self-sustaining oscillations (Marotzke 1990) and aperiodic fluctuations (Weaver and Sarachik 1991) have also been found. Frankignoul and Hasselmann(1976) have shown that adding stochastic terms to the forcing, representing the high frequency atmospheric variations, also leads to oceanic variability on long time scales and a red spectrum of oceanic variables. This may reflect the role of the ocean as an integrator of heat. All these results strongly indicate the crucial role of the ocean for the explanation of observed long-term variations in the climate system.

The water mass distributions and the associated ocean circulation are forced by fluxes of heat, salt and momentum. These fluxes depend both on

the state of the ocean and on the atmosphere and reflect the fact that the systems are truly coupled. Atmospheric models are frequently run with prescribed ocean surface temperatures. This can be justified as the atmospheric time-scale is so much shorter than the one for the ocean. For ocean models this may cause serious problems as the atmosphere adjusts very rapidly to changes in the ocean circulation. Nevertheless many experiments with ocean models have been performed using either restoring or mixed boundary conditions. However the stability of stationary states, the existence of multiple steady states and the observed variability in ocean models appear to depend crucially on the type of boundary conditions applied. This is one of the principle difficulties when modelling long term variations in the ocean. The strong ocean-atmosphere coupling induces atmospheric variations as a response to fluctuations in ocean surface temperatures. These variations will affect the interface fluxes, leading to positive and or negative feedbacks.

It is possible to run coupled general circulation models, but this is still extremely expensive and prevents a detailed exploration of the mechanisms behind the slow fluctuations in the ocean. An alternative approach could be to develop an atmospheric model that is simple and yet describes adequately the crucial atmospheric feedback processes to the ocean. This may improve our knowledge of the coupling processes and in addition may provide the possibility of seriously studying the ocean dynamics on long time-scales. We have developed a coupled atmosphere ocean sea-ice model (ECBILT) with the intention to fullfill the above requirements.

As a first step the model will be used to study the interaction between the stormtracks in the atmosphere with the area of convection at high latitudes in the ocean. As shown by Lenderink and Haarsma (1994), the ocean circulation may exhibit a multiplicity of stationary states, which are connected to the area where convection occurs. With relatively small perturbations in the surface fluxes it appears possible to trigger transitions from one stationary state to another. This leads to decadal oscillations in the strength of the thermohaline circulation and possibly decadal climate fluctuations. In particular we will study the role of the hydrological cycle in the coupling between stormtrack and thermohaline circulation.

This report describes the three components of the model, i.e. the atmosphere, the ocean and the sea-ice model. It runs on present generation workstations. For the Power Indigo Silicon Graphics workstation the coupled model uses 0.2 hr cpu time for 1 yr time integration.

2 Outline of the model

The climate model contains three separate subsystems (atmosphere, ocean and sea-ice), which exchange heat, moisture and momentum. Before discussing the subsystems in detail we will discuss the cycles of these three quantities.

2.1 Heat cyle

The heat source for the climate model is the solar radiation. The solar radiation at the top of the atmosphere goes through a seasonal cycle. Diurnal variations are neglected. The incoming solar radiation are daily averaged values. This radiation is partly used for heating of the atmosphere by direct absorption and for heating of the surface. The surface releases its heat by the exchange of latent and sensible heat with the atmosphere and by the emission of long wave radiation. The emitted terrestrial longwave radiation is absorbed by the atmosphere. The atmosphere also emits longwave radiation which is partly reabsorbed by the earth. If the climate system is in thermal equilibrium, the emitted longwave radiation at the top of the atmosphere will balance the net incoming solar radiation. In the atmosphere there is transport of sensible and latent heat by convection, diffusion and winds. For the solid surface it is assumed that there is no heat transport, which implies a zero heat capacity. In the oceans the heat is transported by convection, diffusion and the ocean currents. The presence of sea-ice, which is formed if the sea-water is colder than -2 ^{o}C, strongly reduces the heat exchange between ocean and atmosphere. It also represents a sink of latent heat.

2.2 Hydrological cycle

The model contains a full hydrological cycle. In the atmosphere the transport of moisture is described by a single equation for the total precipitable water content between the surface and 500 hPa. Sources and sinks for atmospheric moisture are evaporation and precipitation respectively. Evaporation over land and sea are described by bulk formulae. The evaporation over land is proportional to the soil moisture content. In case of snow or sea-ice cover the evaporation is replaced by sublimation. Precipitation occurs when the relative humidity becomes larger than a certain treshold value (usually 80%).

Clouds are prescribed according to the observed zonal mean climatology. Changes in soil moisture are due to precipitation of rain, evaporation, melting of snow and run-off. Run-off occurs when the soil moisture content exceeds a maximum value. The run-off is added to the ocean. The net fresh-water flux for the ocean is composed of: precipitation, evaporation and run-off. In case of sea-ice cover the freshwater flux for the ocean is modified by, brine rejection, sea-ice melt and snow (on top of the sea-ice) melt.

2.3 Momentum cycle

In the atmosphere momentum is generated by differential diabatic heating. It is dissipated by internal friction and by the transfer of momentum from the atmosphere to the earth. The ocean currents are driven by surface winds and by density differences resulting from differential surface fluxes of heat and freshwater. The momentum of the oceans is dissipated by internal friction. Because it is assumed that variations in the momentum budget of the earth can be neglected on the time scales of interest, the momentum of the earth is taken to be constant. The momentum cycle is therefore not closed.

2.4 Short description of the subsystems

The atmospheric model is a spectral quasi-geostrophic model with three vertical levels. The horizontal resolution is T21. The dynamical part was developed by Molteni (see Marshall and Molteni 1993). The physical parameterization is similar to the one described by Held and Suarez (1978). It contains bulkformulae for the exchange of sensible and latent heat and simple schemes for short and long wave radiation. An advection equation for moisture containing sources and sinks describes the hydrological cycle. The cycle is closed by equations for soil moisture, snow melt and river runoff. Cloud cover is prescribed.

The ocean model is an extension of the model described in Lenderink and Haarsma (1994). The model has spherical geometry and a realistic land-sea mask. The horizontal resolution is 5.6 degrees and it has 12 vertical levels. It has a flat bottom. The barotropic and baroclinic components are solved separately. This reduces the computational cost significantly. Convective adjustment occurs in case of unstable stratification.

The sea-ice model is a zero layer thermodynamic model (Semtner 1976). Ice dynamics is not included.

3 Atmospheric model

The description of the atmospheric model is composed of a description of the dynamics and of a description of the physical parameterisations. The third paragraph contains the land surface processes, while the time integration is discussed in paragraph four.

3.1 Dynamics

In the first part of this section the dynamic equations are given. In the second part the discretisation of these equations is discussed. The third part treats the parameterisation of the heating and dissipation terms.

3.1.1 Equations

The dynamical behaviour of the atmospheric model is governed by the quasi-geostrophic equations. These are derived from the primitive equations under the assumption of small Rossby number $R_l = \frac{U}{fL} < 1$, where U and L are the characteristic velocity and length scales of the motion respectively and $f = 2\Omega\sin(\phi)$ the coriolis parameter. Ω is the angular velocity of the earth, ϕ is latitude and λ is longitude. The basic equations are given below. For a detailed derivation the reader is referred to Holton (1979) and Pedlosky (1979). The equations in isobaric coordinates are:

- The vorticity equation:

$$\frac{\partial \zeta}{\partial t} + \mathbf{V}_\psi \cdot \nabla(\zeta + f) + f_o D + k_d \nabla^8 \zeta = -F_\zeta \qquad (1)$$

  where $\zeta = \nabla^2\psi$ is the vertical component of the vorticity vector, ψ is the streamfunction, $\mathbf{V}_\psi$ is the rotational component of the horizontal velocity, D is the divergence of the horizontal wind, f is the coriolisparameter, f_o is f at 45 deg North and South, $k_d\nabla^8\zeta$ is a highly scale

selective diffusion and F_ζ contains the ageostrophic terms in the vorticity equation. It reads:

$$F_\zeta = \mathbf{V}_\chi \cdot \nabla(\zeta + f) + \zeta D + \omega \frac{\partial \zeta}{\partial p} + \mathbf{k} \cdot \nabla\omega \times \frac{\partial \mathbf{V}_\psi}{\partial p} \tag{2}$$

where $\mathbf{V}_\chi$ is the divergent component of the horizontal wind. Estimates of F_ζ will be used to represent the effect of the ageostrophic circulation on the tendency of the geostrophic vorticity.

- The first law of thermodynamics:

$$\frac{\partial}{\partial t}\left(\frac{\partial \psi}{\partial p}\right) + \mathbf{V}_\psi \cdot \nabla\left(\frac{\partial \psi}{\partial p}\right) + \frac{\sigma}{f_o}\omega + k_d\nabla^8\left(\frac{\partial \psi}{\partial p}\right) + k_R\left(\frac{\partial \psi}{\partial p}\right) = -\frac{RQ}{f_o p c_p} - F_T \tag{3}$$

where $\sigma = -\frac{\alpha}{\theta}\frac{\partial \theta}{\partial p}$ is the static stability, α is specific volume, θ is the potential temperature, $\omega = \frac{dp}{dt}$ is the vertical velocity in isobaric coordinates, k_R is a Rayleigh damping coefficient, R is the gasconstant, p is pressure, c_p is the specific heat for constant pressure, Q is the diabatic heating and F_T is the advection of temperature by the ageostrophic wind.

$$F_T = \mathbf{V}_\chi \cdot \nabla\left(\frac{\partial \psi}{\partial p}\right) \tag{4}$$

In the derivation of equation 3 use has been made of the hydrostatic equation relating the temperature T and the geopotential ϕ:

$$T = -\frac{p}{R}\frac{\partial \phi}{\partial p} \tag{5}$$

and the 'geostrophic' relation relating ϕ and ψ

$$\phi = f_o \psi \tag{6}$$

- The continuity equation:

$$D + \frac{\partial \omega}{\partial p} = 0 \tag{7}$$

Equations (1), (3) and (7) can be combined into one equation for the quasi-geostrophic potential vorticity q by eliminating ω and D:

$$\frac{\partial q}{\partial t}+\mathbf{V}_\psi\cdot\nabla q+k_d\nabla^8(q-f)+k_R\frac{\partial}{\partial p}\left(\frac{f_o^2}{\sigma}\frac{\partial\psi}{\partial p}\right)=-\frac{f_oR}{c_p}\frac{\partial}{\partial p}\left(\frac{Q}{\sigma p}\right)-F_\zeta-\frac{\partial}{\partial p}\left(\frac{f_oF_T}{\sigma}\right) \tag{8}$$

where q is defined as:

$$q=\zeta+f+f_o^2\frac{\partial}{\partial p}\left(\sigma^{-1}\frac{\partial\psi}{\partial p}\right) \tag{9}$$

3.1.2 Ageostrophic forcing

The divergent component of the wind can be computed diagnostically from the vorticity equation or the thermodynamic equation once we know the tendency. From $\mathbf{V}_\chi$ and ω the ageostrophic terms F_ζ and F_T can be computed. In the computation of the tendency $\frac{\partial\psi}{\partial t}$ from the potential vorticity equation 8 we will use as a first guess the values of F_T and F_ζ as determined in the previous timestep. The tendency $\left(\frac{\partial\psi}{\partial t}\right)_t$ is computed and the corresponding divergent circulation diagnosed. Computing F_T and F_ζ from this divergent circulation a new estimate for $\left(\frac{\partial\psi}{\partial t}\right)_t$ is derived. We iterate until $\left(\frac{\partial\psi}{\partial t}\right)_t$ has converged. In practice the adjustments in $\left(\frac{\partial\psi}{\partial t}\right)_t$ after the first iteration are substantially smaller than 10%. After 2 iterations the adjustments are smaller than 1%. We usually run the model without iterating.

We have included the ageostrophic terms in order to be able to simulate the Hadley circulation quantitatively correctly. This has enormous consequences for the strength and position of the jetstream and for the transient eddy activity.

3.1.3 Model discretisation

The model is spectral with horizontal truncation T21. The vertical discretisation is shown in fig. 1. The model has three vertical levels, at 800 hPa, 500 hPa and 200 hPa respectively, on which the potential vorticity equation (8) is applied. In deriving the discretized form of eq.(8) , we start from eq.(1) and eq.(3). The vorticity equation (1) is applied at these three levels, whereas the temperature equation (3) is applied at the intermediate levels 650 hPa

and 350 hPa. In the subsequence of this paper these layers will be labeled from 0 to 5 according to figure 1. At the top of the atmosphere ($p = 0$ hPa) the rigid lid condition $\omega = 0$ is applied. The lower boundary condition for ω is:

$$\omega_s = -\rho_s g(\frac{C_d}{f_o}\zeta_s - \mathbf{V}_{\psi \mathbf{s}} \cdot \nabla h) \tag{10}$$

where $\omega_s = \left(\frac{dp}{dt}\right)_s$ is the vertical motion field and ζ_s the vorticity at the top of the boundary layer, for which we take ζ at 800 hPa, C_d is the surface drag coefficient, ρ_s is the density at the surface and $\mathbf{V}_{\psi \mathbf{s}}$ the rotational velocity at the surface, h is the orographic height. Using these boundary conditions, and the equations (1) and (3) in discretized form at the above mentioned levels we can derive the discretized equivalent of eq.(8) at the levels 1, 3 and 5 respectively. They read as follows:

$$\begin{aligned}
\frac{\partial q_1}{\partial t} &= -\mathbf{V}_{\psi \mathbf{1}} \cdot \nabla q_1 - k_d \nabla^8 (q_1 - f) + \lambda_2^{-2} k_R \Delta\psi_{13} + forc_1 \\
\frac{\partial q_3}{\partial t} &= -\mathbf{V}_{\psi \mathbf{3}} \cdot \nabla q_3 - k_d \nabla^8 (q_3 - f) + \lambda_4^{-2} k_R \Delta\psi_{35} - \lambda_2^{-2} k_R \Delta\psi_{13} + forc_2 \\
\frac{\partial q_5}{\partial t} &= -\mathbf{V}_{\psi \mathbf{5}} \cdot \nabla q_5 - k_d \nabla^8 (q_5 - f) - \lambda_4^{-2} k_R \Delta\psi_{35} + forc_3
\end{aligned} \tag{11}$$

where

$$\begin{aligned}
q_1 &= \zeta_1 - \lambda_2^{-2} \Delta\psi_{13} + f \\
q_3 &= \zeta_3 + \lambda_2^{-2} \Delta\psi_{13} - \lambda_4^{-2} \Delta\psi_{35} + f \\
q_5 &= \zeta_5 + \lambda_4^{-2} \Delta\psi_{35} + f
\end{aligned} \tag{12}$$

and

$$\begin{aligned}
forc_1 &= \gamma_{cor}(-\frac{\lambda_2^{-2} R \Delta p}{f_o p_2 c_p} Q_2 - \lambda_2^{-2} \Delta p F_{T2}) - F_{\zeta 1} \\
forc_2 &= \gamma_{cor}(-\frac{\lambda_4^{-2} R \Delta p}{f_o p_4 c_p} Q_4 + \frac{\lambda_2^{-2} R \Delta p}{f_o p_2 C_p} Q_2 - \lambda_4^{-2} \Delta p F_{T4} + \lambda_2^{-2} \Delta p F_{T2}) - F_{\zeta 3} \\
forc_3 &= \gamma_{cor}(\frac{\lambda_4^{-2} R \Delta p}{f_o p_4 c_p} Q_4 + \lambda_4^{-2} \Delta p F_{T4}) - F_{\zeta 5} + \frac{f_o \omega_s}{\Delta p}
\end{aligned} \tag{13}$$

$\Delta p = 300 hPa$, $\Delta\psi_{13} = \psi_1 - \psi_3$, $\Delta\psi_{35} = \psi_3 - \psi_5$, λ_2 and λ_4 are the Rossby radii of deformation appropriate to the 200-500 hPa layer and the 500-800 hPa layer respectively:

$$\lambda_2^{-2} \equiv \frac{f_o^2}{\sigma_2(\Delta p)^2}$$
$$\lambda_4^{-2} \equiv \frac{f_o^2}{\sigma_4(\Delta p)^2}$$

The heating terms Q_2 and Q_4 and the advection of temperature with the ageostrophic wind F_{T2} and F_{T4} enter the potential vorticity equation via the stretching of planetary vorticity ($f\frac{\partial\omega}{\partial p}$). Keeping f equal to f_o in the stretching term generates a discontinuity across the equator, because f_o changes sign. We have pragmatically avoided the discontinuity by multiplying the Q and F_T terms in the forcing equations (13) by $\gamma_{cor} = f/f_o$.

In the computation of ω_s we assume that $\zeta_s = \zeta_5$ and $\mathbf{V}_{\psi\mathbf{s}} = \mathbf{V}_{\psi\mathbf{5}}$ Finally we remark that for the computation of the transport of tracers, like moisture, ω_i is deduced from the discretized thermodynamic equation by:

$$\omega_i = \frac{\Delta p \lambda_i^{-2}}{f_o}\left(\frac{\partial \Delta\psi_i}{\partial t} + \mathbf{V}_{\psi\mathbf{i}} \cdot \nabla\Delta\psi_i + k_d\nabla^8\Delta\psi_i + k_R\Delta\psi_i - \frac{\Delta pRQ_i}{f_o p_i c_p} - \Delta pF_{Ti}\right)$$

for $i = 2$ and $i = 4$, where $\Delta\psi_i = \psi_{i-1} - \psi_{i+1}$. The horizontal divergence is computed from ω by numerical integration from the surface.

3.1.4 Damping timescales

For the Ekman dissipation we assume

$$k_E = \frac{\rho_s g C_D}{f_o} = \tau_E^{-1}(1 + \alpha_1 LS(\lambda,\phi) + \alpha_2 FH(h)), \qquad (14)$$

where τ_E is the Ekman damping time scale, which is assumed to be 6 days. The expression between brackets parameterizes the effect of surface roughness and the orographic height. The fraction of land within a grid box is given by LS and

$$FH = 1 - exp(-h/1000)$$

The α_i are constants: $\alpha_1 = \alpha_2 = 0.5$.
For the scale selective diffusion coefficient we take:

$$k_D = \tau_D^{-1} a^8 (21 * 22)^{-4}, \tag{15}$$

where a is the earth radius. This results in a damping time scale of wavenumber 21 of $\tau_D = 2$ days.

The Rayleigh damping represents the effect of temperature relaxation between the levels 1, 3 and 5. For the damping coefficient we have taken $k_R = \tau_R^{-1}$, with $\tau_R = 30$ days.

3.2 Physics

The diabatic heating in the atmosphere is caused by the radiative heating, the release of latent heat and the exchange of sensible heat with the earth. In the following paragraphs we will discuss the parameterisations of these processes. The release of latent heat is strongly connected with the transport of moisture and convection, which will be treated in two separate paragraphs.

3.2.1 Vertical profiles

The lowest atmospheric level on which the vorticity is computed is 800 hPa. The atmospheric boundary layer is not explicitly resolved by the model. Therefore, in order to compute the heat, moisture and momentum fluxes between the atmosphere and the earth, assumptions about the temperature, moisture and wind profiles in the boundary layer have to be made. For the temperature we assume a linear profile in the logarithm of pressure from the surface to 200 hPa, isothermal above 200 hPa and passing through the computed temperatures at 650 and 350 hPa. The temperature at pressure p is then given by:

$$T(p) = T_4 + \gamma \ln(p/p_4)$$

where

$$\gamma = \frac{T_2 - T_4}{\ln(p_2/p_4)}$$

The temperature just above the surface will be denoted as T_*. The actual surface temperature will be denoted as T_s. Over land T_s is the land surface temperature and over sea the temperature of the upper ocean layer. In case of snow or sea-ice cover it is the snow or sea-ice temperature respectively.

Using the vertical profile of the temperature expressed above, the ideal gas law and hydrostatic equilibrium, T_* is given by

$$T_* = \sqrt{T_{500}^2 - \frac{2\gamma g}{R}(z_h - z_{500})} \tag{16}$$

where z_h is the topographic height, z_{500} the height of the 500 hPa pressure level and T_{500} the temperature at 500 hPa. The 500 hPa geopotential height is computed from the streamfunction at 500 hPa by solving the linear balance equation. In the atmospheric model, the global mean value of 500 hPa geopotential height is undetermined. We assume a value of 5500 m which is in accordance with the standard atmosphere.

The temperature T_* computed in this way is considered as the atmospheric temperature at anemometer level. For the moisture we assume that the relative humidity is constant from the surface to the 500 hPa level. The surface wind $\vec{V}_s$ is estimated by $0.8(\vec{V}_{\psi 5} + \vec{V}_{\chi 5})$.

For the computation of the diabatic heating the atmosphere is divided in two layers between the surface and 500 hPa, and 500 hPa and 200 hPa. They will be denoted the lower (subscript l) and the upper (subscript u) layer respectively.

3.2.2 Radiation

The radiation is divided in two bands: a shortwave radiation band for the solar radiation and a longwave radiation band for the terrestrial radiation.

The absorption and scattering of shortwave radiation is simplified by neglecting multiple scattering. Fig. 2 shows the simplified radiation scheme. Reflection occurs only at the top of the atmosphere and the surface. Absorption in the atmosphere is parameterized as a fraction of the incoming solar radiation at the top of the atmosphere. The reflected sunligth from the surface is reemitted into space.

The incoming solar radiation Q_o is given by

$$Q_o = S_c \cos(Z),$$

where S_c is the solar constant and Z the daily averaged zenith angle. This is computed by:

$$\cos(Z) = \frac{1}{2\pi}\left(\sin(\phi)\sin(\delta)(HA_1 - HA_2)\right)$$

where ϕ, δ, and HA are latitude, declination and hour angle, respectively (Sellers 1965). HA_1 is the time of sunrise and HA_2 the time of sunset.

The absorption of shortwave radiation SW in the upper and lower layer is given by:

$$\begin{aligned} SW_u &= (1 - r_a)\chi_u Q_o, \\ SW_l &= (1 - r_a)(1 - \chi_u)\chi_l Q_o, \end{aligned}$$

where r_a is the reflection coefficient at the top of the atmosphere and χ_u and χ_l the absorption coefficients of the upper and lower layer respectively.

The absorption of SW at the surface is given by:

$$SW_s = (1 - r_s)(1 - \chi_u)(1 - \chi_l)(1 - r_a)Q_o,$$

where r_s is the surface albedo. r_a, χ_u and χ_l are given as a function of latitude and time of the year. The surface albedo r_s is determined by the surface characteristics. The different types of surface are land, snow, ocean and sea- ice respectively. The albedos for each surface type are a function of latitude and time of the year.

The longwave radiation (LW) at the interfaces of the layers (see figure 2) is computed according to the parameterization of Held and Suarez (1978). Assuming a constant profile for moisture and the trace gases, they parameterized the LW as computed by the radiation scheme of the GCM of the GFDL. The LW was parameterized as a function of the vertical structure of the potential temperature:

$$LW_i = a_i(\bar{\theta}) + b_i(\bar{\theta})\hat{\theta} + c_i(\bar{\theta})\Delta T,\ i = 1,\ 2$$

where $\bar{\theta} = 0.5(\theta_2 + \theta_4)$, $\hat{\theta} = 0.5(\theta_2 - \theta_4)$ and $\Delta T = T_* - T_s$. LW_i represents the different components of the longwave radiation as depicted in fig. 2. The downward flux of LW at the surface LW_s is computed with the parameterization of Holtslag and van Ulden (1983):

$$LW_s = C_1\sigma T_*^6 + C_2 f_c$$

where σ is the Stefan-Boltzmann constant and f_c the cloud coverage. The coefficients $C_1 = 9.35 * 10^{-6} K^{-2}$ and $C_2 = 60\ Wm^{-2}$ are empirical constants. For f_c we have taken the zonal averaged values from Peixoto and Oort (1993). The LW emitted by the earth surface is σT_s^4

3.2.3 Moisture

Changes in the specific humidity are described by a single equation for the total precipitable water content between the surface and 500 hPa. Above 500 hPa the atmosphere is assumed to be completely dry.

$$\frac{\partial q_a}{\partial t} = -\nabla_3 \cdot (\vec{V}_a q_a) + E - P,$$

where q_a is the total precipitable water content between the surface and 500 hPa, $\vec{V}_a$ the transport velocity for q_a, E evaporation and P precipitation. For the horizontal component of $\vec{V}_a$ 60 % of the sum of the geostrophic and ageostrophic velocity at 800 hPa ($\vec{V}_5$) is taken. The vertical component of $\vec{V}_a$ is ω_{500}, which is calculated as the average of ω_2 and ω_4.

Because above 500 hPa the atmosphere is assumed to be dry, moisture which is advected through this plane by the vertical velocity ω is removed by precipitation which falls through the underlying layer.

Below 500 hPa precipitation occurs when $q_a > 0.8 q_{max}$ where q_{max} is the vertically integrated saturation specific humidity below 500 hPa. Water is precipitated in case of undersaturation because the precipitation criterion applies for gridbox averaged values for which complete saturation never will occur. q_{max} is computed from

$$q_{max} = \frac{1}{\rho_w} \int_{p_0}^{500hPa} q_s(T,p) \frac{dp}{g}. \tag{17}$$

where p_0 denotes the surface pressure and ρ_w is the density of water. The surface pressure p_0 is computed from

$$p_0 = p_4 \exp(\frac{T_* - T_4}{\gamma})$$

The saturation specific humidity q_s is computed from the saturation vapour pressure e_s

$$q_s(p) = \frac{\epsilon e_s}{p},$$

where

$$e_s(T) = 611.2 \exp(17.67 \frac{T - 273}{T - 29.66})$$

is an approximate Clausius-Clapeyron relationship for e_s (Stull, 1988) and

$$\epsilon = \frac{m_v}{m_d},$$

where m_v and m_d are the moleculair weigths of water vapour and dry air respectively.

The integral (17) can be evaluated analytically and expressed in terms of exponential integrals. Since these exponential integrals are numerically rather expensive, q_{max} is tabulated for a range of values for the temperatures at 350 hPa, 650 hPa and the temperature above the surface. The values of q_{max} are linearly interpolated inside the temperature intervals.

The relative humidity r is assumed to be constant throughout the lower atmospheric layer and is given by

$$r = \frac{q_a}{q_{max}}$$

By definition then, the specific humidity q as a function of pressure is given by

$$q(p) = r q_s(p).$$

The amount of precipitation is given by:

$$\Delta q_a = \frac{(q_a - 0.8 q_{max})}{1 + \frac{r \rho_w L_c g}{c_p \Delta p_l} \frac{dq_{max}}{dT_4}},$$

where L_c is the latent heat of condensation. The precipitation is released during one time step Δt, so the rate of precipitation P is $\frac{\Delta q_a}{\Delta t}$. The term in the denominator is a correction to account for the heating of the lower atmospheric layer by the condensation of water vapour. The derivative of

q_{max} with respect to the temperature of the lower atmospheric layer T_4 is estimated from the tabulated values of q_{max} by finite differences.

The release of latent heat due to precipitation is $L_c \Delta q_a$. If the surface temperature is below $0°C$, we assume that the precipitation is in the form of snow which implies that the phase change is from water vapor to ice so that L_c is replaced by the latent heat of sublimation L_s.

The evaporation over sea is given by

$$E_{sat} = \rho_a C_d |V_s| (q_s(p_0, T_s) - q(p_0, T_*))$$

where ρ_a is the air density, C_d is the drag coefficient and $|V_s|$ the absolute value of the wind speed at anemometer level. Over land the evaporation is reduced proportional to the soil moisture content (see section 3.3.2).

3.2.4 Convective adjustment

For unsaturated situations convective adjustment occurs when the vertical temperature gradient $\frac{dT}{dz}$ exceeds the dry adiabatic lapse rate

$$\Gamma_d = \frac{g}{c_p}.$$

In saturated situations the moist adiabatic lapse rate

$$\Gamma_s = \Gamma_d \left[\frac{1 + \frac{L_c q_s}{RT}}{1 + \frac{\epsilon L_c^2 q_s}{c_p R T^2}} \right]$$

at 500 hPa is used.

After the convective adjustment it is again checked if $q_a > 0.8 q_{max}$. If this is the case there will be additional precipitation. In the remainder this will be called *convective* precipitation in contrast to *dynamic* precipitation which is due to supersaturation caused by large scale geostrophic motions. The latent heat due to this convective precipitation is released in the lower layer and is directly used to compute a new temperature distribution. For this new temperature distribution the convective adjustment procedure is applied again. This starts an iterative process which stops if the stratification is stable and $q_a < 0.8 q_{max}$. This happens usually within three iterations.

3.2.5 Sensible heat

The surface flux of sensible heat SH is given by

$$SH = \rho_a c_p C_d |V_s| (T_s - T_*)$$

.

3.2.6 Diabatic heating

The diabatic heating is computed from the various diabatic processes as follows:

$$\begin{aligned} Q_2 &= \frac{g}{c_p \Delta p_u}(LW_2 - LW_1 + SW_u + LH_u) \\ Q_4 &= \frac{g}{c_p \Delta p_l}(\sigma T_s^4 - LW_s - LW_2 + SW_l + LH_l + SH) \end{aligned}$$

See fig. 2 for the symbols of the different terms in the longwave radiation. LH_u and LH_l refer to the release of latent heating in the upper and lower layer respectively. Here the latent heat release is due to dynamic *and* convective rain. The sensible heat SH is released in the lower layer. Δp_u and Δp_l are the layer depths of the upper (300 hPa) and lower (500hPa) layer respectively.

3.2.7 Temperature

From the distribution of the quasi-geostrophic potential vorticity q the horizontal temperature distribution at level 2 and 4 can be computed from eq.(12), eq.(6) and eq.(5). Using eq.(6) relating ϕ and ψ, however, resulted in problems along the equator because of the discontinuity in f_o at the equator. We therefore used the linear balance equation instead.

$$\nabla^2 \Phi = \nabla \cdot (f \nabla \psi).$$

Because of the Laplacian in eq.(12) q determines ψ except for a constant value. This implies that the horizontal globally averaged temperature cannot be computed from the potential vorticity distribution. The global mean temperature for each layer is therefore directly computed from the diabatic heating:

$$\frac{\partial T_{Mi}}{\partial t} = \frac{Q_{Mi}}{c_p}$$

for $i = 2, 4$, where T_{Mi} and Q_{Mi} are the globally averaged values for temperature and diabatic heating at layer i respectively. In the diabatic heating, however, *only* the component due to the dynamic rain is used. The convective adjustment procedure, including the temperature increase due to convective rain, modifies the values of T_{Mi}. The new values of T_{Mi} are computed directly after the convective adjustment procedure by globally averaging the new temperature distribution.

3.3 Land surface processes

3.3.1 Surface temperature

We compute the land surface temperature T_s from the assumption of zero heat capacity of the surface, which implies a zero net heat flux F_a between the atmosphere and the land surface:

$$F_a \equiv -SW_s - LW_s + LH_s + SH - \sigma T_s^4 = 0 \tag{18}$$

where LH_s is the cooling of the surface due to evaporation:

$$LH_s = E_w L_c \tag{19}$$

E_w is the evaporation over land and is discussed in the next section. If $T_s < 0^oC$, L_c in eq.(19) is replaced by L_s, the latent heat of sublimation. Because LH_s and SH also depend on T_s, T_s is solved iteratively.

3.3.2 Soil moisture

A source for soil moisture is the precipitation of rain. As already mentioned in section 2, If $T_s > 0^oC$ the precipitation is in the form of rain (P_r). If the surface temperature is below 0°C the precipitation is in the form of snow (P_s). Snow will become a source of soil moisture in case of melting of the snow cover (M_s). Sinks of soil moisture are evaporation (E_w) and run-off (R_o). Horizontal and vertical transport of soil moisture is neglected. The equation for the total soil moisture content W is therefore:

$$\rho_w \frac{\partial W}{\partial t} = P_r + M_s - E_w - R_o$$

where ρ_w is the density of water.

If snow covers the soil, no evaporation of soil moisture is allowed. It is assumed that the rain falls through the snow. The land surface has a uniform soil moisture capacity W_{max}. The soil moisture evaporation is linearly dependend on the soil moisture content:

$$E_w = \frac{W}{W_{max}} E_{sat},$$

where E_{sat} is the evaporation over sea (see section 3.2.3). If W becomes larger than W_{max}, W is reset to W_{max} and the difference added to the river runoff R_o. If $W < W_{max}$, $R_o = 0$.

3.3.3 Snow cover

Accumulation of snow occurs if $T_s < 0$ in case of precipitation. Ablation of snow is caused by snow melt and evaporation. The resulting equation for the snow depth H_s is:

$$\rho_s \frac{\partial H_s}{\partial t} = P_s - E_s - M_s$$

where E_s is the sublimation of snow. ρ_s is the density of snow. Snow melt occurs if T_s computed in eq.(18) is above 0^oC. The rate of snow melt is computed by

$$M_s = \frac{F_{0a}}{L_f},$$

where F_{0a} is the net heat flux between snow and atmosphere computed by eq.(18) for $T_s = 0^oC$. L_f is the latent heat of fusion of snow.

3.4 Time integration

The equations (11) for the quasi-geostrophic potential vorticity are solved using a fourth-order Runga-Kutta scheme. The physics is computed on grid-points at the gaussian grid. The equations for atmospheric moisture, globally averaged temperature, soil moisture content and snow cover are integrated using a forward scheme. The time step is 4 hrs.

4 Ocean model

4.1 Basic equations

The model equations are given by the heat and salt budgets, continuity equation, a quadratic equation of state, the hydrostatic approximation, and the horizontal momentum equation.

- Heat and salt budget:

$$\frac{\partial T}{\partial t} + \nabla \cdot (uT) + \frac{\partial}{\partial z}(wT) = \kappa_h \nabla^2 T + \kappa_v \frac{\partial^2 T}{\partial z^2} + F^T + D^T \quad (20)$$

$$\frac{\partial S}{\partial t} + \nabla \cdot (uS) + \frac{\partial}{\partial z}(wS) = \kappa_h \nabla^2 S + \kappa_v \frac{\partial^2 S}{\partial z^2} + F^S + D^S \quad (21)$$

  where T is temperature and S is salinity. F and D represent the atmospheric forcing and deep water formation process respectively. κ_h and κ_v are the horizontal and vertical eddy diffusivities respectively.

- Continuity equation:

$$\frac{\partial w}{\partial z} + \nabla \cdot u = 0 \quad (22)$$

- Equation of state:

$$\rho(S,T) = \rho_m + k_S S + k_T (T - T^m)^2 \quad (23)$$

  where $\rho_m = 1001,3263$ kg m^{-3} K^{-2}, $k_S = 0.7739$ kg m^{-3} per promille, $k_T = -0.00471$ kg m^{-3}, $T^m = 265.42$ K. The units of T and S are Kelvin and PSU (promille) respectively. This equation of state is a fit, linear in S and quadratic in T, to the UNESCO formula (1981) and is designed to represent the horizontal pressure gradients reasonable well. The pressure dependency has been ignored.

- Hydrostatic equation:

$$\frac{\partial p}{\partial z} = -\rho g \quad (24)$$

- Horizontal momentum equations:

$$\begin{aligned} \frac{\partial u}{\partial t} - fv &= \frac{-1}{\rho_o a \cos\phi}\frac{\partial p}{\partial \lambda} + \nu\nabla^2 u + \frac{\partial}{\partial z}(\kappa\frac{\partial u}{\partial z}) \\ \frac{\partial v}{\partial t} + fu &= \frac{-1}{\rho_o a}\frac{\partial p}{\partial \phi} + \nu\nabla^2 v + \frac{\partial}{\partial z}(\kappa\frac{\partial v}{\partial z}) \end{aligned} \tag{25}$$

where ν and κ are the horizontal and vertical eddy viscosities respectively. The kinematic boundary condition at $z = 0$ is the rigid lid approximation $w = 0$. Using the hydrostatic equation p can be written as

$$p(\lambda, \phi, z) = p_s(\lambda, \phi) + p^*,$$

where p_s is the surface pressure and

$$p^* = \int_z^0 \rho(\lambda, \phi, z) g dz$$

4.2 Atmospheric forcing

The ocean circulation is forced by surface fluxes of heat, freshwater and momentum. The heat flux between ocean and atmosphere is computed in the same way as the heatflux between atmosphere and land and is given by F_a (see section 3.3.1 equation (18)). Here T_s is the temperature of the ocean surface layer. The total freshwater flux into the oceans is:

$$F_w = P - E + R \tag{26}$$

where P is precipitation, E evaporation and R is river run-off.

For computing the river run-off, the land surface is divided in a number of basins BL_i representing the drainage areas of the major rivers. The integrated run-off of a land basin BL_i is added to an ocean basin BO_i representing the coastal seas adjacent to a river delta. The correspondence between land and ocean basins is one to one: each land basin corresponds with one ocean basin. Fig. 3 displays the distribution of the land and ocean basins respectively. The transfer of run-off from land basins to ocean basins occurs without time delay: each time step the total run-off of a land basin is added to the corresponding ocean basin.

For forcing the ocean model the freswater flux is transformed into a virtual salt flux:

$$\frac{\partial S_s}{\partial t} = -\frac{S_s F_w}{h_s}$$

where S_s and h_s are surface salinity and depth of the surface layer respectively. Because the salinity changes induced by the freshwater flux are small in respect to the total salinity, the virtual salt flux can be approximated by:

$$\frac{\partial S_s}{\partial t} = -\frac{S_s F_w}{h_s}. \tag{27}$$

This formulation of the virtual salt flux in equation (27) does not guarantee that the global mean virtual salt flux is zero in case of a zero global mean fresh water flux. The imbalances generated during one year of the integration are compensated by adding a constant correction term during the following year. Replacing S_s in the r.h.s. of equation (27) by the mean salinity of the ocean S_o, would eliminate the problem. This, however, generates unrealistic virtual salt fluxes in places where the surface salinity strongly deviates from the mean salinity, which is the case at high latitudes.

Formation of sea-ice causes an additional salt flux into the ocean due to brine rejection. Melting of sea ice causes a negative virtual salt flux. The virtual salt flux B due to the growing and melting of sea-ice is given by:

$$B = -\frac{\rho_i}{\rho_o}\frac{(S_s - S_i)}{h_s}\frac{\partial h_i}{\partial t} \tag{28}$$

where h_i is the ice thickness, S_i the salinity of sea-ice and ρ_i and ρ_o are the mean densities of sea-ice and sea-water respectively. In case of sea-ice cover the precipitation will be in the form of snow and will contribute to the accumulation of snow over the sea-ice. However if the sea-ice or the snow on top of the sea-ice is melting, the precipitation is in the form of rain and is assumed to fall through the sea-ice layer.

The atmospheric windstress is computed by the following drag law:

$$\vec{\tau} = -\rho_a C_d |V_s| \vec{V_s} \tag{29}$$

4.3 Splitting in barotropic and baroclinic modes

The momentum equations are split into a barotropic (depth averaged) and a baroclinic part (deviation from barotropic velocity). The rigid lid approximation eliminates fast external gravity waves and makes the barotropic part of the momentum equations divergence free. This enables to introduce a streamfunction. Taking the curl of the barotropic momentum equation results in a prognostic equation for the streamfunction in which the surface pressure is eliminated. The baroclinic momentum equation also does not contain a dependency on the surface pressure.

The barotropic mode is defined by:

$$\bar{u} = \frac{1}{H}\int_{-H}^{0} u dz \tag{30}$$

$$\bar{v} = \frac{1}{H}\int_{-H}^{0} v dz \tag{31}$$

where H is the depth of the ocean basin. A barotropic streamfunction ψ can be defined:

$$\begin{aligned} a^{-1}\partial_\phi \psi &= -H\bar{u} \\ (a\cos\phi)^{-1}\partial_\lambda \psi &= H\bar{v} \end{aligned}$$

Integrating the momentum equations vertically we get:

$$\begin{aligned} \frac{\partial \bar{u}}{\partial t} - f\bar{v} &= \frac{-1}{\rho_o a H \cos\phi}\int_{-H}^{0}(\frac{\partial p}{\partial \lambda} + \nu\nabla^2\bar{u})dz + \frac{\kappa}{H}\frac{\partial u}{\partial z}\,|_{-H}^{0} \\ \frac{\partial \bar{v}}{\partial t} + f\bar{u} &= \frac{-1}{\rho_o a H}\int_{-H}^{0}(\frac{\partial p}{\partial \phi}dz + \nu\nabla^2\bar{v})dz + \frac{\kappa}{H}\frac{\partial v}{\partial z}\,|_{-H}^{0} \end{aligned}$$

With a constant depth H the $\int$ and the ∇^2 operator can be reversed. The windstress is given by:

$$\kappa\frac{\partial u}{\partial z}\,|_{z=0} = \frac{\tau_x}{\rho_o}$$

$$\kappa\frac{\partial v}{\partial z}\,|_{z=0} = \frac{\tau_y}{\rho_o}$$

The bottom stress is neglected.
Using the definition of the barotropic streamfunction ψ we get:

$$-a^{-1}\frac{\partial}{\partial t}(\frac{\partial \psi}{\partial \phi}) - f(a\cos\phi)^{-1}\partial_\lambda \psi = \frac{-1}{\rho_o a\cos\phi}\int_{-H}^{0}\frac{\partial p}{\partial \lambda}dz - a^{-1}\nu\nabla^2\partial_\phi\psi + \frac{\tau_x}{\rho_o}$$

$$(a\cos\phi)^{-1}\frac{\partial}{\partial t}(\frac{\partial \psi}{\partial \lambda}) - fa^{-1}\partial_\phi \psi = \frac{-1}{\rho_o a}\int_{-H}^{0}\frac{\partial p}{\partial \phi}dz + \nu\nabla^2(a\cos\phi)^{-1}\partial_\phi\psi + \frac{\tau_y}{\rho_o}$$

By taking the curl of this set of equations an equation for the barotropic streamfunction ψ is obtained. This operation eliminates not only the surface pressure dependency but also the density dependency if H is assumed to be constant. The Laplacian friction term is replaced by a linear friction term.

$$\nu\nabla^2\bar{u} = -\kappa_s\bar{u}$$

A Laplacian friction would have given an ∇^4-term in the barotropic streamfunction equation. This term cannot be resolved accurately by the coarse grid (An artificially high diffusion constant has to be chosen in order to resolve the boundary current). In addition, the solution of the barotropic streamfunction by direct elimination is hardly feasable on a global grid if a ∇^4-term is used.
Eliminating the local time derivative results in the Stommel equation for a wind driven barotropic flow:

$$\kappa_s\nabla^2\psi + \frac{\partial_\phi f}{a^2\cos\phi}\frac{\partial\psi}{\partial\lambda} = \frac{\vec{k}\cdot\nabla\times\vec{\tau}}{\rho_o} \tag{32}$$

The baroclinic mode is defined by:

$$\hat{u} = u - \bar{u} \tag{33}$$

This eliminates the surface pressure p_s

$$\frac{\partial\hat{u}}{\partial t} - f\hat{v} = \frac{-1}{\rho_o a\cos\phi}[\frac{\partial p^*}{\partial\lambda} - \frac{1}{H}\int_{-H}^{0}\frac{\partial p^*}{\partial\lambda}dz] + \nu\nabla^2\hat{u} + \frac{\partial}{\partial z}(\kappa\frac{\partial\hat{u}}{\partial z}) \tag{34}$$

4.4 Discretization

The system is discretized on a Arakawa B-grid. The horizontal position of the scalar and vector points is shown in fig. 4. On the scalar points the temperature, salinity, density, and the barotropic streamfunction are computed. On the vector points the horizontal velocity components u and v are computed. The model has 12 vertical layers of 30, 50, 80, 140, 250, 350, 400, 450, 500, 550, 600 and 600 m. The vertical velocity w is computed at the intersection between two layers. The atmospheric forcing is added to the two top layers.

For the Arctic ocean and a few shelf seas like the Mediterranean sea and the sea of Ochotsk, the momentum equations (25) are onmitted and in the tracer equations (20) and (21) only the diffusive terms and atmospheric forcing are retained. This is done because of the coarse resolution of the ocean model which inhibits a faithfull simulation of the ocean currents in these small seas. The depth of these diffusive "lakes" is set at 1000 m. They exchange heat and salt with the ocean through diffusivity. The diffusion coefficients for the diffusion in the "lakes" and for the exchange with the ocean can be chosen independently of the diffusion coefficient of the ocean model. The location of the lakes is depicted in fig. 3.

4.4.1 Boundaries

The land-sea boundary is put on the vector points. The no slip condition and the no normal flow condition are employed, i.e. the velocities u and v are set to zero on the land-sea boundary. There is no flux of heat and salt across the boundary. For the horizontal advection this is achieved by the no normal flow condition. For horizontal diffusion the normal derivative of the tracer is set to zero.

For the barotropic mode the value of the streamfunction ψ is imposed (zero except for islands) for those vector-points which are surrounded by at least one boundary vector point (see fig. 4). Consequently, scalar points near the boundary at sea exist where the boundary value of the barotropic streamfunction is imposed. This is consistent with the no slip/no normal flow condition.

Due to the absence of bottom topography the Antarctic circumpolar current will be strongly underestimated. In order to correct for this deficiency

the boundary value of the streamfunction ψ at Antarctica is set to generate a barotropic mass transport of 100 Sv through the Drake passage in the absence of wind forcing.

4.5 Time integration

4.5.1 Barotropic mode

The barotropic mode is not integrated in time but is solved as an equilibrium response to a given wind forcing. Hereto, eq.(32) is discretized on the scalar-points. This yields a linear set of equations $A\psi = b$. The matrix A is a sparse band matrix and is only dependent on the geometry of the problem and does not change during the time integration. This set, including the boundary conditions, can be solved directly by elimination. Hereto, a LU-decompostion of A is made once, and the system $Lb' = b$, $U\psi = b'$ is solved every timestep. (This procedure can only be applied if A is a matrix with a relatively small bandwidth. A ∇^4 operator in the barotropic vorticity equation doubles the bandwidth compared to the ∇^2 operator and makes a direct solvage of the barotropic vorticity equation by elimination hardly feasable on a workstation)

4.5.2 Baroclinic mode

In the model, the baroclinic mode is defined different from eq.(33). Instead the kth-baroclinic mode in the model is defined by:

$$\hat{u}_k = u_k - u_{k-1} \tag{35}$$

where u_k is the velocity at level k. The used definition of the baroclinic mode facilitates the computations in the model for this mode. The equations for the kth-baroclinic mode become

$$\begin{aligned} \frac{\partial \hat{u}_k}{\partial t} - f\hat{v}_k &= \frac{-1}{\rho_o a \cos\phi}\frac{\partial p_\rho}{\partial \lambda} + \nu\nabla^2\hat{u}_k + M_v \\ \frac{\partial \hat{v}_k}{\partial t} + f\hat{u}_k &= \frac{-1}{\rho_o a}\frac{\partial p_\rho}{\partial \phi} + \nu\nabla^2\hat{v}_k + M_v \end{aligned} \tag{36}$$

Here, M_v denotes vertical diffusion and

$$p_\rho = \frac{\rho_k + \rho_{k-1}}{2}\frac{h_k + h_{k-1}}{2}$$

where it is assumed that the density varies linearly between the two levels. The timestepping is forward for the diffusive terms and backward for the coriolis term.

4.5.3 Distorted physics approach

The coupled system of denstity and momentum equations is capable of producing internal gravity waves. The first internal gravity mode has a typical velocity of 3 m/s. This would limit the size of the timestep in the tracer (T and S) equations to half a day. In order to slow down the phase speed of these waves an asynchronous (K. Bryan, 1984) timestepping procedure can be applied. This procedure is commonly employed in ocean models. Basically, this procedure consist of integrating an alternative momentum equation together with the unaltered tracer equations:

$$\begin{aligned} \frac{\partial \hat{u}_k}{\partial t_d} - f\hat{v}_k &= \frac{-1}{\rho_o a \cos\phi}\frac{\partial p}{\partial \lambda} + \nu\nabla^2\hat{u}_k + M_v \\ \frac{\partial \hat{v}_k}{\partial t_d} + f\hat{u}_k &= \frac{-1}{\rho_o a}\frac{\partial p}{\partial \phi} + \nu\nabla^2\hat{v}_k + M_v, \end{aligned}$$

where $t_d = t/\alpha$ and $\alpha > 1$. This alternative system can be considered a distorted physics system. In the distorted physics system the velocity adjusts slower to the density field compared to the undistorted system. For the distorted system it can be shown that the internal gravity modes and the baroclinic Rossby modes slow down a factor $\sqrt{\alpha}$ and α respectively (Bryan, 1984). The large scale slowly changing geostrophic mode, important for climate studies, is largely unaffected by the distorted physics approach. The Rossby number is the ratio between the local derivative and the coriolis term

$$R_o = \frac{u^*/t^*}{fu^*}.$$

Typical values for the large scale ocean circulation are $t^* = 1$ year, $f = 10^{-4}s^{-1}$ and $u^* = 10^{-1}m/s$, yielding $R_o = 10^{-3}$. Given these scales it might be expected that, even with $\alpha = 100$, a geostrophic flow in the distorted physics system remains mainly geostrophic. The distorted physics method, however, should be handled with care if fast small scale changes are considered.

Modelling the distorted physics system is easily achieved by taking a smaller (factor α) timestep in the momentum equation of the undistorted system.

4.5.4 Heat and salt budgets

For the timestepping of the heat and salt budget equations a Leapfrog method is used for horizontal advection and a forward time stepping procedure for horizontal diffusion, vertical diffusion, and vertical advection.

4.5.5 Deep water formation

To represent the deep water formation process a convective adjustment procedure is employed after each timestep. Starting from the uppermost two levels it is checked if they are unstably stratified and in that case the two levels are completely mixed for T and S. The mixing process conserves the total heat and salt content of the two levels. Next, the same procedure is applied to the second and the third level. This process is repeated until the lowest level is reached. Note that this procedure does not garantee complete stability of the whole column. In order to decrease the remaining unstability the whole convective procedure can be repeated a few times. One should keep in mind that the time scale of the convective process is dependent on the time step of the budget equations.

5 Sea-ice

Sea-ice is formed if the ocean temperature drops below -2 °C. Sea-ice affects the heat budget of the ocean and the atmosphere by strongly reducing the heat exchange between those two subsystems. The salinity budget of the ocean is affected by sea-ice by means of brine rejection and melt water. The effect of sea-ice on the momentum transfer between atmosphere and ocean is neglected.

The sea-ice model is based on the zero layer model of Semtner(1976). This model computes the thickness of sea-ice from the thermodynamic balances at the top and the bottom of the ice. A schematic diagram of the ice model is depicted in fig. 5. The ice model consists of a single layer of sea ice with a

variable thickness H_i. On top of the ice there is a layer of snow with thickness H_s.

At equilibrium there exists a balance of heat fluxes at the top and the bottom of the ice layer:

$$F_a - F_s = 0 \tag{37}$$
$$F_b - F_s = 0 \tag{38}$$

where F_a is the atmospheric heat flux at the top of the ice, F_s the conductive heatflux through the ice and snow layers and F_b the heat flux between the ocean and the bottom of the ice.

The conductive heat flux F_s is assumed to be linearly dependent on the ice thickness and the tempearture difference between the top and the bottom of the ice layer:

$$F_s = \frac{k_s k_i}{k_s H_i + k_i H_s}(T_b - T_s) \tag{39}$$

where H_i is the ice-layer thickness, H_s the snow-layer thickness and k_i the thermal conductivity of ice, k_s the thermal conductivity of snow and T_b the bottom temperature of the ice-layer. T_b is equal to the freezing point of sea water.

The oceanic heat flux F_b is assumed to be proportional to the temperature difference between the mixed layer and the bottom of the ice slab:

$$F_b = b(T_o - T_b) \tag{40}$$

where T_o is the ocean temperature in the mixed layer beneath the ice and b the exchange coefficient.

The flux balances (37) and(38) are maintained by changing T_s and by melting and ablation at the top and bottom of the ice layer respectively.

If the computed value of T_s is > 0 ^{o}C, it is reset to 0 ^{o}C. The resulting imbalance between F_a and F_b will be used to melt the ice or snow.

The change in the ice thickness is given by

$$\rho_i \frac{dH_i}{dt} = \frac{(F_a - F_s)}{L_f} + \frac{(F_s - F_b)}{L_f} \tag{41}$$

where ρ_i is the density of sea ice. The first term at the r.h.s. is due to melting, the second term due to ablation or accretion at the bottom of the ice. If the sea-ice is covered with snow this will melt first

$$\rho_s \frac{dH_s}{dt} = \frac{(F_a - F_s)}{L_f} \tag{42}$$

where ρ_s is the density of snow.

6 The coupled model

The time step of the atmospheric model is 4 hrs, whereas the ocean model has a time step of 1 day, implying 6 atmosphere time steps for one ocean time step. During these 6 time steps the ocean surface is kept constant. The fluxes of heat, moisture and momentum across the ocean surface are integrated during this period and used during the next time step of the ocean model. The time step of the sea-ice model is chosen to be equal to that of the atmosphere model.

The horizontal discretization of grid points in zonal direction (5.625 degrees) is the same for the scalar gridpoints (T, q, S) of the atmosphere and ocean model. In meridional direction the discretisation is slightly different because of the difference between a regular lat-lon and a Gaussian grid. In this case the values have to be interpolated. The wind speed of the atmosphere has to be interpolated to the vector points of the Arakawa-B grid of the ocean model. The sea-ice model is computed at the scalar points of the ocean model. The land-sea mask is shown in figure 4.

References

[1] Bjerknes, J., 1964: Atlantic air-sea interactions. Adv. Geophysics., 10, 1-82.

[2] Broecker, W.S., D.M. Peteet and D. Rind, 1985: Does the ocean-atmosphere system have more than one stable mode of operartion? Nature, 315, 21-26.

[3] Bryan, F., 1986: High-latitude salinity effects and interhemispheric thermohaline circulation. Nature, 323, 301-304.

[4] Bryan, K., 1984: Accelerating the convergence to equilibrium of ocean climate models. J. Phys. Oceanogr., 14, 666-673.

[5] Frankignoul, C. and K. Hasselmann, 1976: Stochasitic climate models, Part 2: Application to sea surface temperature anomalies and thermohaline variability. Tellus, 29, 289-305.

[6] Held, I.M. and M.J. Suarez, 1978: A two-level primitive equation atmosphere model designed for climate sensitivity experiments. J. Atmos. Sc., 35, 206-229

[7] Holton, J.R., 1979: An introduction to Dynamic Meteorology. International Geophysics series, volume 23, second edition. Academic Press, New York.

[8] Holtslag, A.A.M. and A.P. Van Ulden, 1983: A simple scheme for daytime estinates of the surface fluxes from routine weather data. Journ. Appl. Meteor., 22, 517-529.

[9] Lenderink, G. and R. J. Haarsma, 1994: Variability and multiple equilibria of the thermohaline circulation associated with deep water formation. J. Phys. Oceanogr., 24, 1480-1493.

[10] Maier-Reimer, E. and U. Mikolajewicz, 1989: Experiments with an OGCM on the cause of the Younger-Dryas. In: oceanography 1988, UNAM Press, Mexico, 87-100.

[11] Manabe , S., and R.J. Stouffer, 1988: Two stable equilibria of a coupled ocean-atmosphere model. J. of Climate, 1, 841-866.

[12] Marotzke, J., 1990: Instabilities and multiple equilibria of the thermohaline circulation. Ber. Inst. Meeresk., Kiel 194, 126pp.

[13] Marotzke, J. and J. Willebrand, 1991: Multiple equilibria of the global thermohaline circulation. J. Phys. Oceanogr.,21, 1372-1385.

[14] Marshall, J. and F. Molteni, 1993: Toward a dynamic understanding of planetray-scale flow regimes. J. Atmos. Sci., 50, 1792-1818

[15] Mikolajewicz, U. and E. Maier-Reimer, 1990: Internal secular variability in an ocean general circulation model. Clim. Dyn. 4, 145-156.

[16] Pedlosky, J., 1979: Geophysical Fluid Dynamics, Springer Verlag, 710 pp.

[17] Peixoto, J.P and A. H. Oort, 1992: Physics of Climate, American Institute of Physics, New York, 520 pp.

[18] Sellers, W.D., 1965: Physical Climatology, University of Chicago, 272 pp.

[19] Semtner, A.J., 1976: A model for the thermodynamic growth of sea-ice in numerical investigations of climate. J. of Phys. Oceanogr., 6, 379-389.

[20] Stocker, T.F. and L.A. Mysak, 1992: Climate fluctuations on the century time-scale: A rewiew of high resolution proxy data and possible mechanisms, Climate Change, 20, 227-250.

[21] Stommel, H., 1961: Thermohaline convection with two stable regimes of flow. Tellus, 46A, 419-432.

[22] Stull, R. B., 1988: An introduction to Boundary Layer Meteorology, Kluwer Academic Publishers, Dordrecht, 666pp.

[23] UNESCO, 1981: Tenth report of the joint panel on oceanographic tables and standards. UNESCO Techn. Papers in Marine Science, vol. 36, UNESCO, Paris, 25pp.

[24] Weaver, A. and E.S. Sarachik, 1991: The role of mixed boubdary conditions in mumerical models of the ocean. J. Phys. Oceanogr., 21, 1470-1493.

7 Figure captions

Fig. 1: Vertical discretisation of the atmosphere model

Fig. 2: Radiation scheme of the atmosphere model

Fig. 3: Land-sea mask, lakes and run-off basins.The lakes are in light shading. The run-off basins are indicated with the corresponding capital letters.

Fig. 4: Horizontal grid of the ocean model

Fig. 5: Schematic representation of the sea-ice model

Figure 1

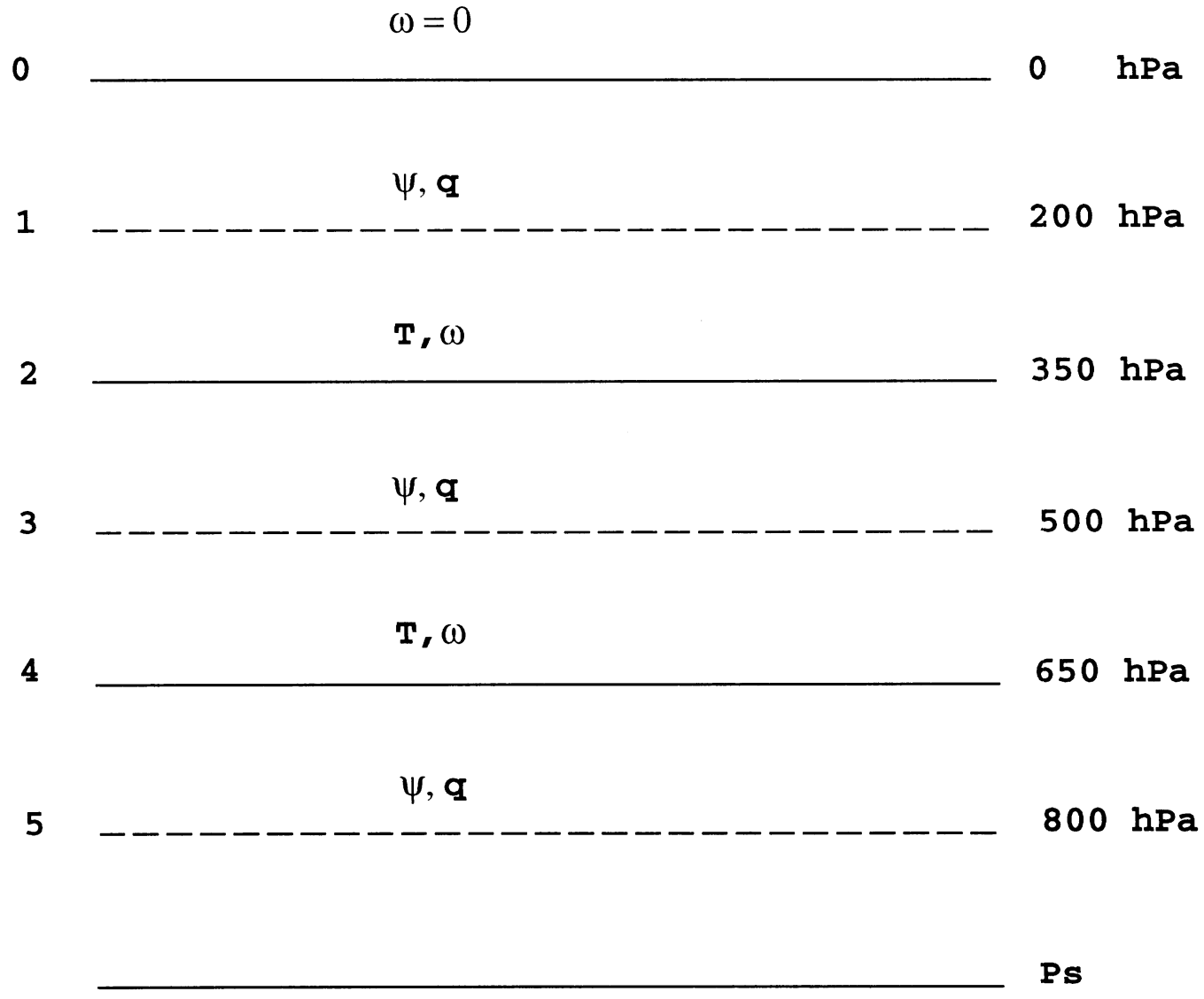
ω = 0
0
0 hPa
ψ, q
1
200 hPa
T, ω
2
350 hPa
ψ, q
3
500 hPa
T, ω
4
650 hPa
ψ, q
5
800 hPa
Ps

Figure 2

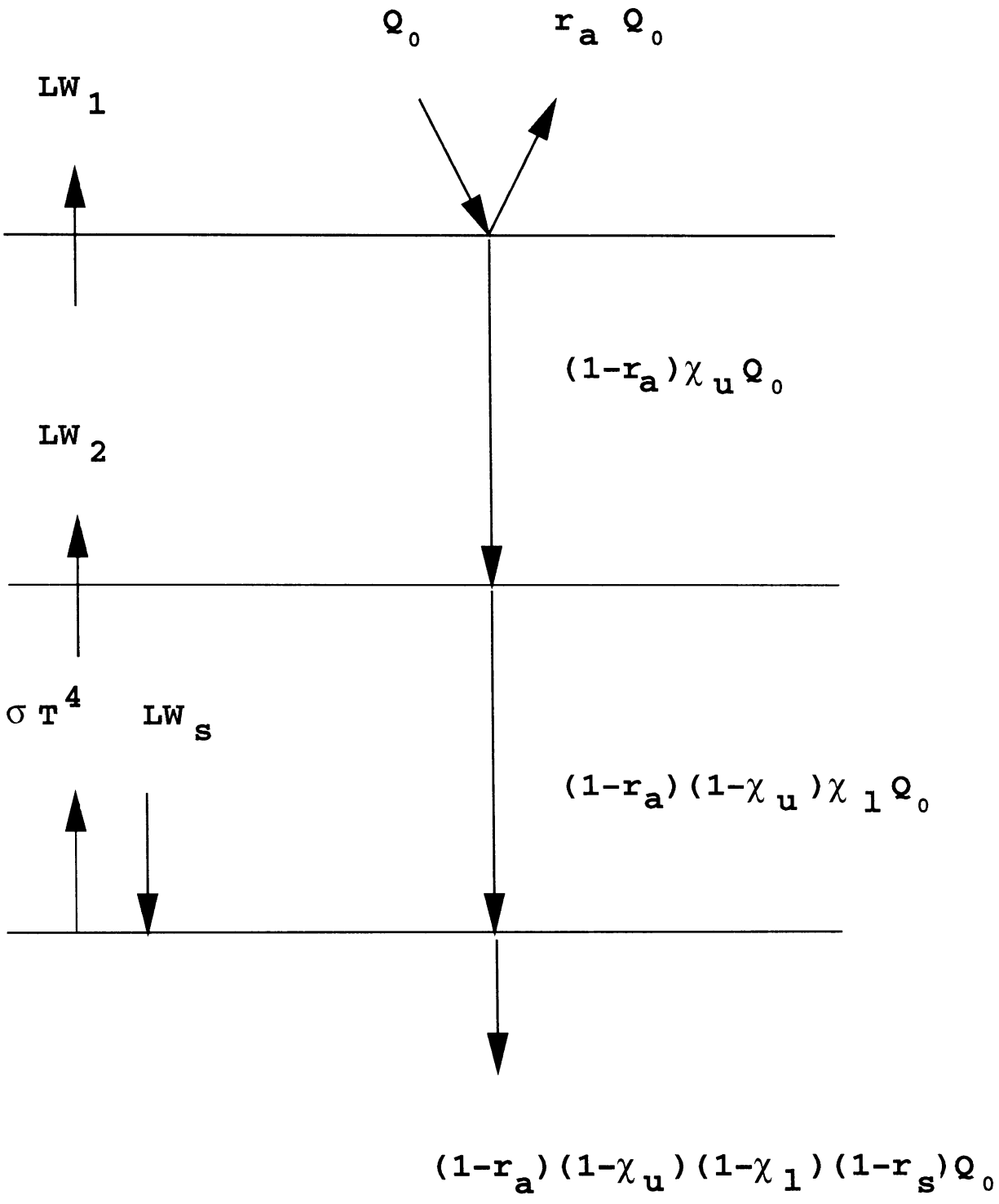
Q_0
$r_a Q_0$
LW_1
$(1-r_a)\chi_u Q_0$
LW_2
σT^4
LW_s
$(1-r_a)(1-\chi_u)\chi_l Q_0$
$(1-r_a)(1-\chi_u)(1-\chi_l)(1-r_s)Q_0$

Figure 3

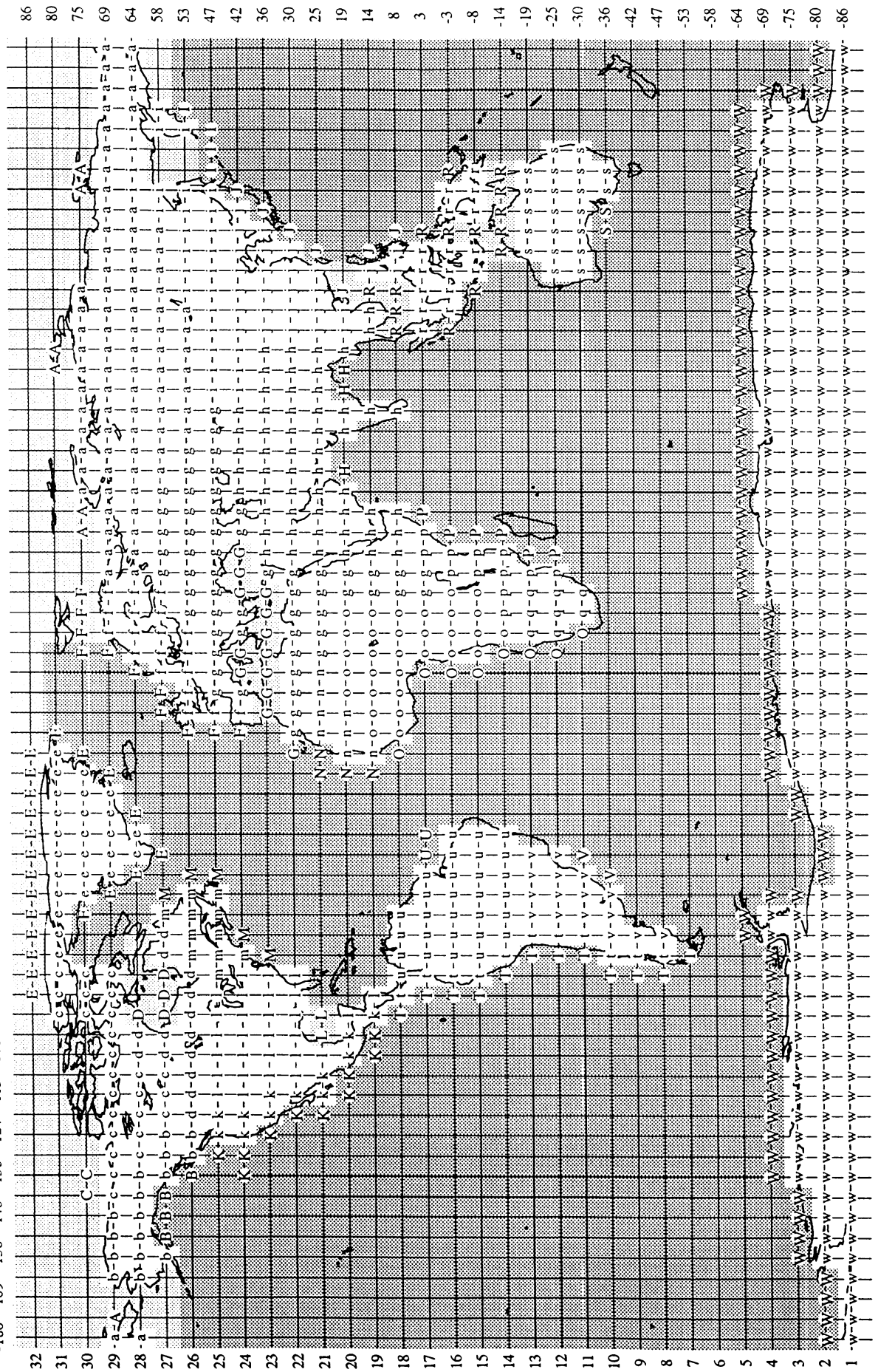

Figure 4

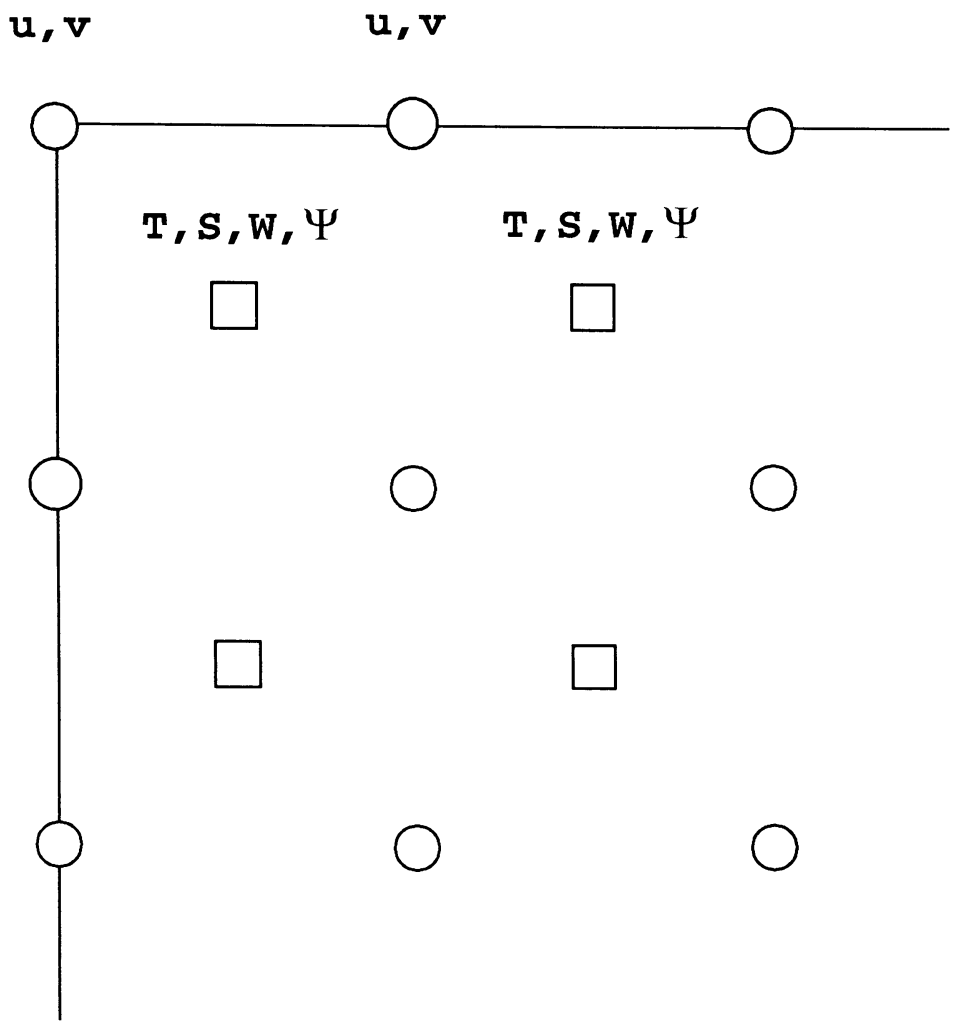

Arakawa B-Grid

Figure 5